Effects of RANS-Type turbulence models on the convective heat loss computed by CFD in the solar two power tower

Available online at www.sciencedirect.com

ScienceDirect

Energy Procedia 49 (2014) 569 – 578

Energy Procedia

SolarPACES 2013

Effects of RANS-Type turbulence models on the convective heat loss computed by CFD in the solar two power tower

R. Zanino[a,*], R. Bonifetto[a], J. M. Christian[b], C. K. Ho[b], L. Savoldi Richard[a]

[a]*Dipartimento Energia, Politecnico di Torino, C.so Duca degli Abruzzi 24, 10129 Torino, Italy*
[b]*Solar Technologies Department, Sandia National Lab P.O. Box, 5800, Albuquerque, NM 87185-1127, USA*

Abstract

The effect of the choice of Reynolds-Averaged Navier-Stokes (RANS) type turbulence closure on the Computational Fluid Dynamics (CFD) prediction of convective heat losses from the Solar Two central receiver is considered in this paper for a simplified receiver geometry approximated by flat panels. Computed convective losses at steady state are ~ 2-3% (1%) of the total power absorbed by the receiver, at high (low) wind speed, depending on the turbulence model chosen. The simulation results are consistent with those of available correlations for rough cylinders, if the macroscopic roughness due to the panel edges is accounted for, as well as with the low speed experimental results, within the respective error bars.

Selection and peer review by the scientific conference committee of SolarPACES 2013 under responsibility of PSE AG.
Final manuscript published as received without editorial corrections.
Keywords: Solar Two; Central receiver systems; Convective heat losses; Computational Fluid Dynamics.

1. Introduction

Computational Fluid Dynamics (CFD) is a powerful tool for the analysis of geometrically complex engineering problems although, of course, the inclusion of more and more details implies progressively increasing computational cost. Therefore, a reasonable trade-off must be found, which typically requires identifying the minimum complexity which still allows capturing with the simulation the main features observed in the experiments.

In the Solar Two power tower, operated using molten salt as the primary (directly heated) fluid and water/vapor

* Corresponding author. Tel.: +39-011-090-4490; fax: +39-011-090-4499.
E-mail address: roberto.zanino@polito.it

Selection and peer review by the scientific conference committee of SolarPACES 2013 under responsibility of PSE AG.
Final manuscript published as received without editorial corrections.
doi:10.1016/j.egypro.2014.03.061

as secondary fluid to produce 10 MWe in a conventional Rankine cycle, the external receiver had a roughly cylindrical shape, approximated by a polyhedron made of 24 heat absorbing panels. Each panel was composed of 32 individual tubes to transport the molten salt, see Fig. 1.

Fig. 1. (a) The Solar Two receiver. (b) Detail of one of the 24 panels of the Solar Two receiver with 32 tubes.

CFD was already used to analyze the issue of heat losses from the Solar Two receiver in previous work performed at Sandia National Lab [1], using a simple 1-equation turbulence model for the air around the receiver (as well as for the molten salt), approximating the panel surface as flat, see Fig. 2a, i.e. neglecting the individual tubes, see Fig. 2b, thanks to the fact that the tube outer diameter (d_{tube} = 2.1 cm) is much smaller than the receiver diameter (D = 5.1 m).

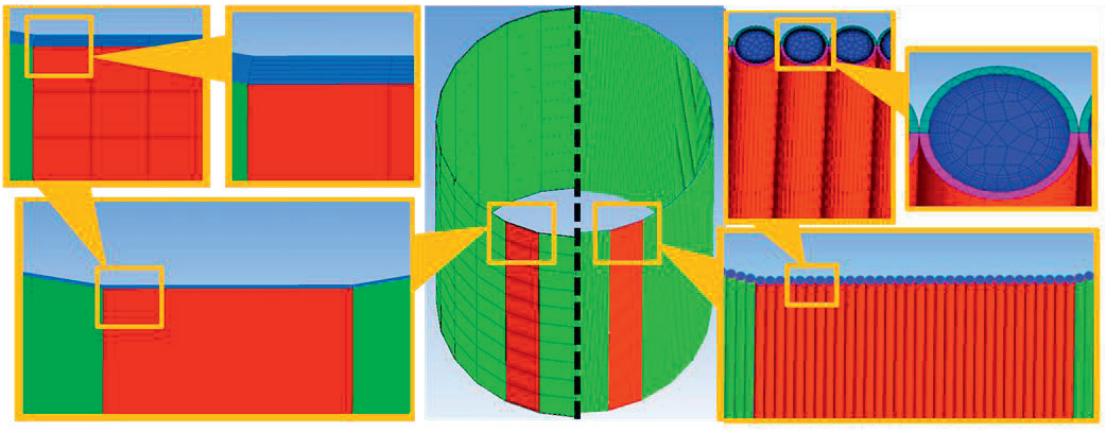

Fig. 2. (a) Left side: Approximate receiver geometry with 24 flat panels, as considered in [1] and in this paper. Right side: Realistic receiver geometry with 24 “rough” panels, made of 32 tubes each. The details of a single panel, of a single tube and of the respective mesh (solid and molten salt domains only) are shown.

Here we present the main results of a CFD analysis of the heat losses from the Solar Two receiver using, as it was done in [1], the ANSYS FLUENT code (release 14.5, vs. release 12.0 used in [1]). We reconsider the work presented in [1], exploring the influence of the choice of the turbulence closure on the computed results. The computed convective heat losses are then compared with the results of available correlations.

Nomenclature

A_{tot}^{panels}	Total area of receiver surface (m^2)
D	Diameter of receiver (m)
d_{tube}	Outer diameter of molten salt tubes (m)
h	Heat transfer coefficient between air and receiver (W/m^2K)
Q_{loss}^{conv}	Convective heat loss (W)
T_{in}^{air}	Inlet air temperature (= free stream/upstream air temperature T_∞) (K)
T_{in}^{salt}	Inlet temperature of molten salt (K)
T_W	temperature of receiver surface (K)
V_{air}	Inlet air speed (m/s)

2. Computational domain and boundary conditions

The computational domain is a hexahedron with a square horizontal base of 30 m side and a height of 36 m. At the center of the domain the receiver is approximated by a hollow polyhedron with 24 sides (5.1 m diameter inscribed cylinder), 6.2 m tall and 0.013 m thick. The other features of the real tower geometry, above and below this cylinder, see Fig.1a, as well as the tube structure of the panels, see Fig. 1b, are neglected in the present version of the model (assuming adiabatic boundary conditions on the two artificially sealed bases of the cylinder), although these features might also play a role in the convective heat loss, see below. On the internal surface of the cylinder adiabatic conditions are assumed.

An imposed mass flow rate of 45 kg/s of molten salt (T_{in}^{salt} = 290 °C) is flowing in each half of the receiver, and the wind is assumed to flow from the west onto the receiver at temperature T_{in}^{air} = 300 K and either relatively high speed V_{air} = 8.98 m/s or relatively low speed V_{air} = 1.35 m/s.

3. Analysis of the receiver with flat panels

The surface heat load (W/m^2) on the receiver computed by the DELSOL code, see Fig. 3a, corresponding to a total incident power of 40 MW, under the assumption of a degradation factor of 85% and a further reduction of 5% to account for the reflective losses from the receiver, with an azimuthal sampling of 30°.

The receiver is modeled in a simplified fashion:

- Each panel is approximated by a single channel of roughly rectangular cross section, sub-divided vertically into 10 partitions, see Fig. 3b, neglecting the pipe structure;
- In each panel only the molten salt is modeled, i.e., the thickness of the walls of the panel/tubes is neglected. The FLUENT "shell conduction" model is adopted, where instead of directly applying the surface heat load, a volumetric heat load (W/m^3) is estimated and applied, dividing the surface heat load by the actual tube wall thickness [2].

The azimuthal and axial distributions of the load on the receiver are obtained by interpolation of the map in Fig. 3a, assuming a constant value on each rectangular tile. Two parallel cooling paths for the molten salt are foreseen, each including the series of 12 panels, see Fig. 3b: the “West” path cools the W1-W6 and then the E7-E12 panels, the “East” path cools the E1-E6 and then the W7-W12 panels [1]. The axial load distribution on the north panel is shown in Fig. 3c.

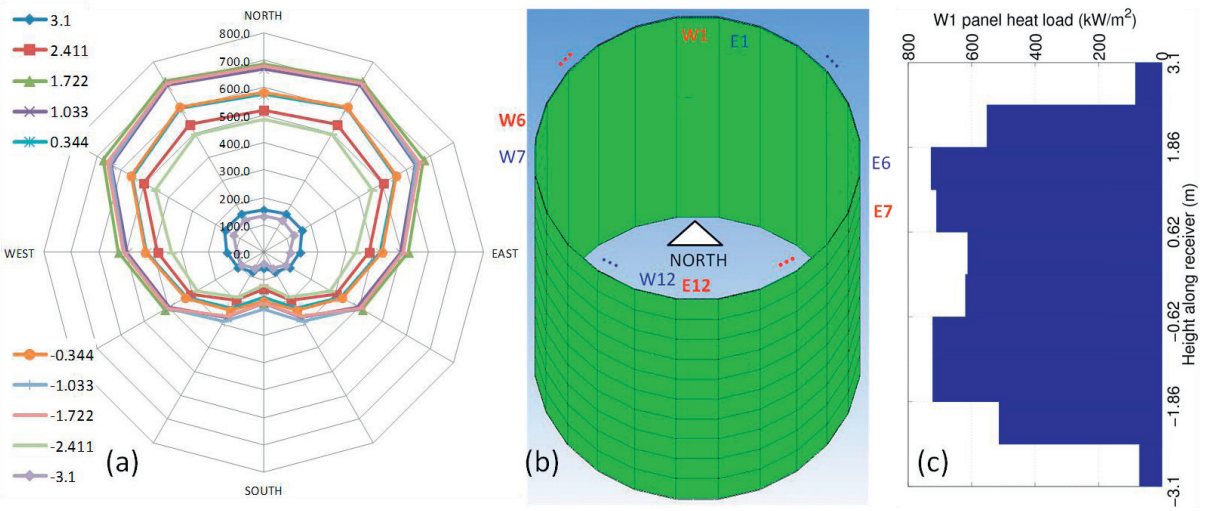

Fig. 3. (a) Radiative load (kW/m^2) on the receiver, as a function of angular position and height along the receiver (m). (b) Simplified geometry of the receiver as adopted in [1]. (c) Axial distribution of the radiative load (kW/m^2) on the receiver W1 (northernmost) panel.

While the analysis in [1] was carried out using the Spalart-Allmaras (SA) turbulence closure [3], here we adopt also two other turbulence models, k-ε RNG (Re-Normalization Group) [4], which is generally available also in other computational environments (e.g., OpenFoam), and k-ω SST (Shear Stress Transport) [5], [6], which is known to be especially suitable for flows with detachment/reattachment patterns as the present one [7]. The effect of this choice on the evaluation of the convective losses from the receiver will be demonstrated.

All three models considered in the paper belong to the family of Reynolds-Averaged Navier-Stokes (RANS)-based turbulence models, where the Reynolds stresses, obtained from a Reynolds averaging of the Navier-Stokes equations, are modelled by a linear constitutive relationship [8]. SA belongs to the sub-class of one-equation models, solving one turbulent transport equation, usually for the turbulent kinetic energy, whereas k-ω SST and k-ε RNG belong to the sub-class of two-equation models, solving also for a second transported variable, like the turbulent dissipation ε or the specific dissipation ω. Of course, it is well known from the analysis of fundamental gas dynamics problems of relevance here, like the external high Reynolds number flow across a cylinder, that the level of approximation implicit in the use of RANS models is rather rough, but on the other hand they allow a relatively cheap solution of several engineering problems, as opposed to other, more sophisticated and accurate methods, like large eddy (LES) or direct numerical simulation (DNS).

The same grid as used in [1] is used also for the two new turbulence models, as all three adopt a so-called enhanced wall treatment [9]. The grid independence of the SA solution was verified in [1].

The steady-state flow and temperature fields are reported in Figs. 4 and 5, respectively. Both fields are shown on the east-west vertical plane passing through the receiver center, and on the equatorial plane of the receiver.

The computed flow field downstream of the receiver shows the flow detachment both at the top and bottom and on the side of the cylinder, qualitatively independent of but quantitatively affected by the choice of the turbulence model, especially the wake region on the back of the receiver, see Fig. 4. The flow on the vertical plane is significantly affected by buoyancy and very similar in the case of SA and k-ω SST. The flow on the equatorial plane is reasonably symmetric, at least with SA and k-ω SST, while asymmetries in the k-ε RNG solution hint at the fact that it could be possibly still evolving. Some spurious effects are noted on the bottom and side boundaries of the computational domain, probably related to the boundary condition imposed there (pressure inlet and outlets, respectively). Notice that the presence of the structures above and below the receiver, not modelled here, could significantly affect this flow field.

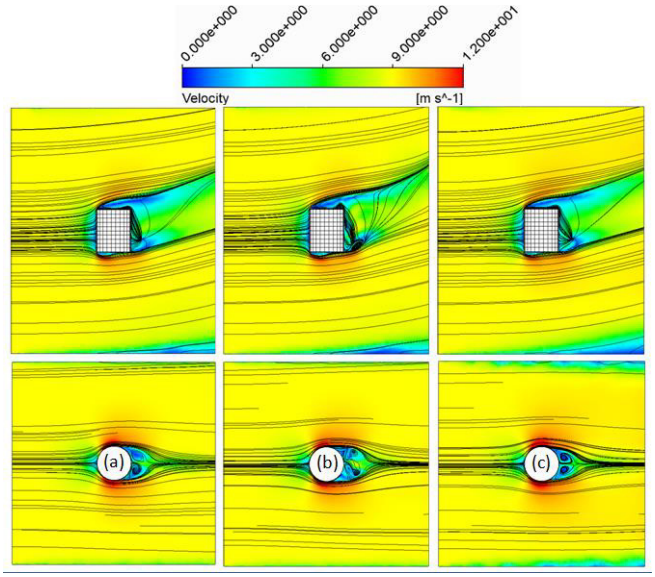

Fig. 4. Computed (ANSYS FLUENT v14.5) air flow field coloured by velocity magnitude (m/s) in the case V_{in}^{air} = 8.98 m/s. Top figures: vertical west-east plane; bottom figures: equatorial plane. Different turbulence models are used: (a) SA as in [1], (b) k-ε RNG, (c) k-ω SST.

The air temperature field in Fig. 5 shows that the volume at high temperature increases as we move from the SA model to the k- ε RNG and eventually to the k-ω SST model, hinting at possibly different computed convective losses in the three cases, see below.

The spatial distribution of the computed convective heat flux from the receiver surface to the air is shown in Fig. 6, which highlights the dramatic influence of the choice of turbulence model on the local computed heat transfer.

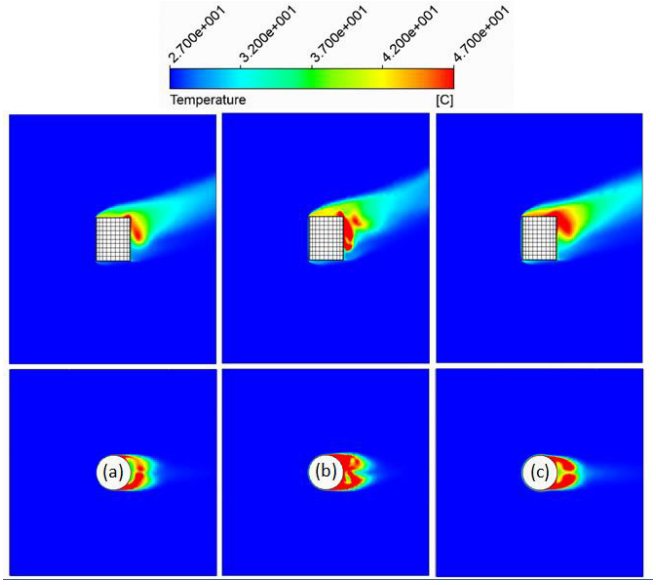

Fig. 5. Computed (ANSYS FLUENT v14.5) air temperature map (°C) in the case V_{in}^{air} = 8.98 m/s. Top figures: vertical west-east plane; bottom figures: equatorial plane. Different turbulence models are used: (a) SA as in [1], (b) k-ε RNG, (c) k-ω SST. Temperatures above 47 °C are represented as if they were equal to 47 °C in order to get a graphical appreciation of the gradients.

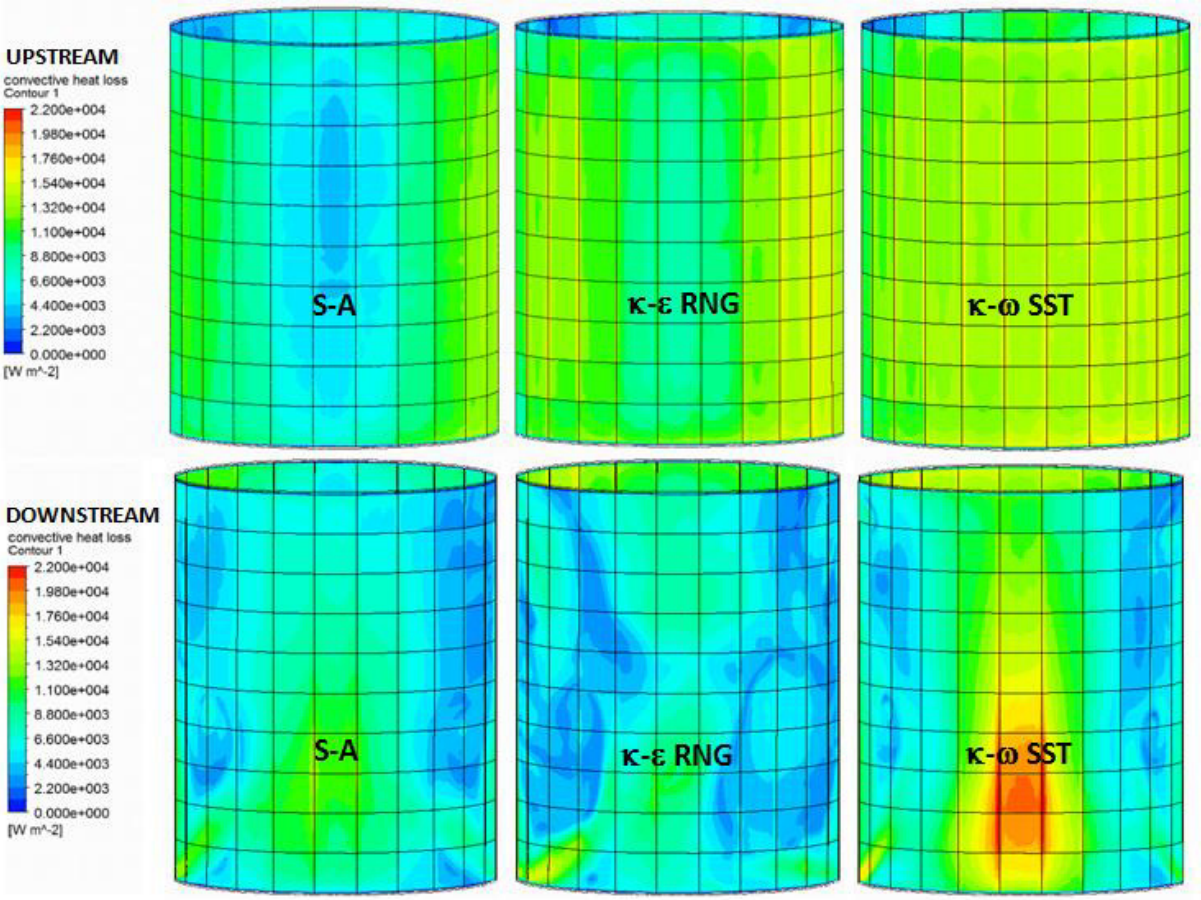

Fig. 6. Computed (ANSYS FLUENT v14.5) convective heat flux map (W/m^2) in the case V_{in}^{air} = 8.98 m/s. Top figures: west face; bottom figures: east face. Different turbulence models are used: (left) SA as in [1], (middle) k-ε RNG, (right) k-ω SST.

Figure 7a shows that in relative terms the k-ω model computes much larger convective losses (surface integral of the heat flux from the receiver to the air, subtracted of the radiative contribution), than those computed with the SA model.

The variation of the computed convective losses as different turbulence models are adopted is consistent with the results in Fig. 7b, where it is shown that the power transmitted to the molten salt decreases when the k-ε RNG and k-ω SST models are used, leading to a lower temperature at the outlet of both East and West cooling paths in the receiver. The slight unbalance (~ 4% difference in the temperature increase between inlet and outlet) between the West/East cooling circuits is also evident in Fig. 7b. It is mainly due to the slight asymmetry of the total radiative load on panels W1+E12 (cooled by West) of ~ 2.7 MW, vs. ~ 3.2 MW on panels W7+E6 (cooled by East), all the rest of the load being symmetrically shared by East and West.

The convective loss expected from the different correlations is computed as

$$Q_{loss}^{conv} = h * A_{tot}^{panels} * (T_W - T_\infty) \quad (1)$$

where A_{tot}^{panels} is the area of the side surface of the receiver in the model, T_W is the average wall temperature (here extracted from the simulations and equal to ~ 780 K) and T_∞ = 300 K is the upstream air temperature. The heat transfer coefficient h is computed accounting for the two contributions of natural convection (h_{nc}) and "forced" convection (h_{fc}) as follows [10]

$$\bar{h} = \left(\overline{h_{fc}}^{a} + \overline{h_{nc}}^{a}\right)^{1/a} \tag{2}$$

where a = 3.2 [11]. The value of h_{nc} in (2) is computed from the Nusselt number Nu_{NC1} (defined using the cylinder height as characteristic length and the air conductivity at T_∞) as

$$Nu_{NC1} = 0.098 Gr^{\frac{1}{3}} \left(\frac{T_w}{T_\infty}\right)^{-0.14} \tag{3}$$

where Gr is the Grashof number:

$$Gr = \frac{g\beta(T_w - T_\infty){L_2}^3}{\nu^2} \tag{4}$$

g is the acceleration of gravity, β is the volumetric thermal expansion coefficient (= 1/ T_∞), L_2 is the height of the receiver, ν is the kinematic viscosity of the air.

The value of h_{fc} in (2) is computed starting from the forced convection Nusselt number Nu_{fc} (where the cylinder diameter is the characteristic length and the air conductivity is evaluated at T_∞), which depends on the roughness of the cylinder surface.

In the case of a smooth cylinder we use for Nu_{fc} the correlation

$$Nu = 0.18\, Re^{0.63}. \tag{5}$$

from [12], or else the Churchill and Bernstein correlation

$$Nu_{FC1a} = 0.3 + 0.488 Re^{0.5} \left[1.0 + \left(\frac{Re}{282000}\right)^{0.625}\right]^{0.8} \tag{6}$$

from [10]. In both cases, the Reynolds number Re is evaluated using the film temperature $T_{film} = 0.5*(T_w + T_\infty)$ for the density, while the viscosity is at T_∞ for consistency (in the CFD simulations the "incompressible ideal gas" assumption is adopted only for the density, while the other properties are assumed to be constant and equal to their value at T_∞).

If, on the contrary, we assimilate the polygonal structure of the receiver to a macroscopic roughness of the order of $(d_{tube}/2)/D \sim 431 \times 10^{-5}$ on top of the smooth cylinder, the convective heat transfer coefficient has been deduced from the Nu_{fc} correlations given in [12] for different Re ranges, considering that here $Re \sim 1.5 \times 10^6$ (if, as explained above, the dynamic viscosity is evaluated at T_{film} and the density at T_{in}^{air}) and interpolating as in [11] the two formulations for relative roughness 300×10^{-5} and 900×10^{-5}

$$Nu_{fc} = K \times 0.0135 \times {Re_{fc}}^{0.89} + (1 - K) \times 0.0455 \times {Re_{fc}}^{0.81} \tag{7}$$

where $K = (431 \times 10^{-5} \_ 300 \times 10^{-5})/ (600 \times 10^{-5})$.

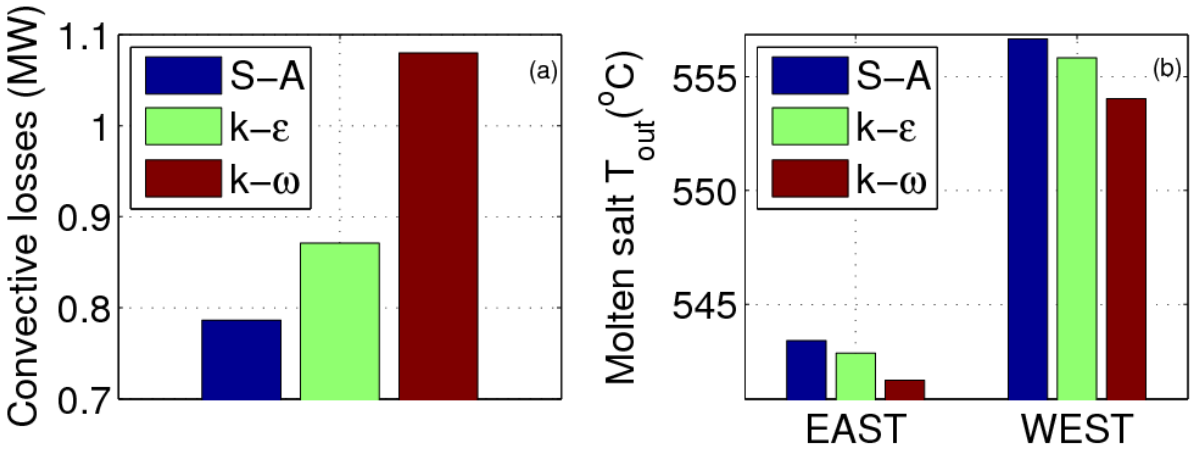

Fig. 7. Effect of different turbulence models in the case V_{in}^{air} = 8.98 m/s. (a) Total convective losses from the receiver. (b) Outlet temperature of the molten salt in the West and East parallel cooling paths.

Notice that correlations for Nu in the case of external flow on polygonal cylinders [10] seem to indicate that already a hexagon is close to the smooth cylinder *at low Re* (below 10^5, say), which would imply the roughness of a 24-sided polygon to be negligible. However, it is also clear that at the much higher Re of interest here, the rough cylinder behaves significantly differently from the smooth cylinder [12].

The comparison between CFD results and correlations in the case of high air speed is presented in Fig. 8, where the evolution of the estimated convective loss during the iterations is reported, together with the predictions of different correlations and the respective error bars. An error bar of ±50% is considered on Nu_{fc} as suggested in [11], while an additional uncertainty of ±40% is applied to the exponent a in (2) [11]. The error bar on Nu_{NC1} is ±40% [11].

First of all Fig. 8 confirms that convergence with the iterations was indeed reached, at least for the SA and k-ω SST. We also see that the CFD simulations predict losses above the smooth cylinder correlations, whereas irrespective of the turbulence closure they are in good agreement, albeit within the rather large error bar, with the results of the "rough" correlation.

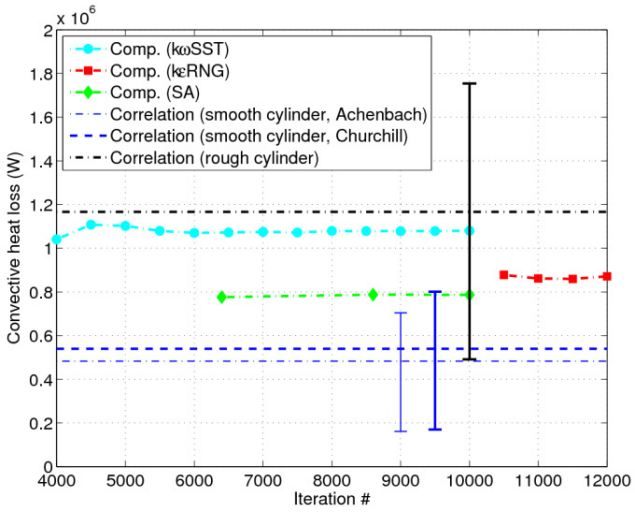

Fig. 8. High wind speed case (8.98 m/s): convective heat loss history computed using different turbulence models, compared to the prediction of different correlations [1].

We now consider the results of the analysis in a case of low wind speed (1.35 m/s), for which experimental data are available (Sep 30-Oct 1 entry in [11]). A simulation with the same heat load as in the high speed case above has been performed (indeed, that load corresponds to the Sep 30-Oct 1 experimental conditions). In this case, natural convection largely dominates the convective heat loss from the receiver.

The CFD simulations have been performed in this case using two different turbulence models (k-ε RNG and k-ω SST), and they are summarized in Fig. 9. In Fig. 9a the experimental total heat loss [11], averaged between the values deduced for Sep. 30, 1997 and Oct. 1, 1997, is reported, together with the associated error bar from [13]. The experimental total heat loss, estimated through the difference between radiative input and molten salt enthalpy increase, including the convective, conductive and radiative contribution, is compared to the simulated total heat loss, accounting however only for the convective and radiative contribution since heat conduction at the receiver boundaries is not included in the model (adiabatic boundary conditions). Considering that the actual conductive loss is estimated to be between 0.5% and 1% of the incident power [1], i.e. ~ 0.2-0.4 MW, the result of the simulation is in good agreement with the experiment, within the error bar, for both turbulence models investigated here.

In Fig. 9b we report the convective loss expected from the correlations above. The forced flow contribution is basically negligible in this case, because although h_{nc} (~ 9 W/m^{2}K) is not huge compared to h_{fc} (~ 2 W/m^{2}K), they combine with the power 3.2 in (2), resulting in a forced convection contribution of less than 1 %. Figure 9b shows that the simulations with both turbulence models are in good agreement with the correlations, within the error bar.

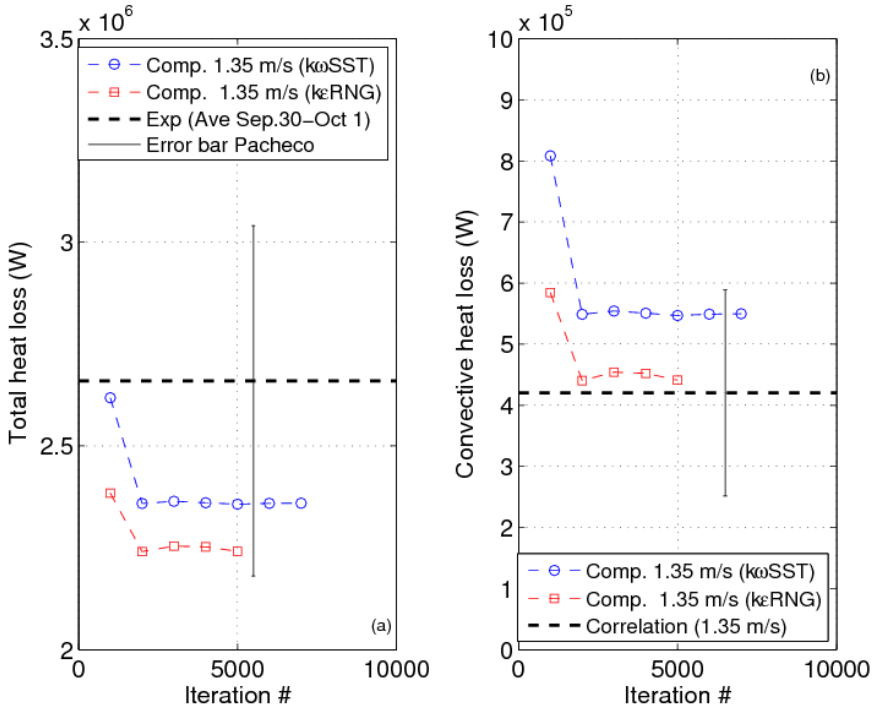

Fig. 9. Low wind speed case: (a) experimental total heat loss, compared to total heat loss history computed using different turbulence models; (b) convective heat loss history computed using different turbulence models, compared to prediction from correlations.

In Table 1 we summarize the results of the comparison between CFD and correlations.

Table 1. Estimated convective heat loss (MW): comparison between CFD, correlations and experiment.

	SA	k-ε RNG	k-ω SST	Smooth cylinder correlations	Rough cylinder correlation
High wind speed (8.98 m/s)	0.79 [a]	0.87	1.08	0.5 ± 0.3	1.18 ± 0.6
Low wind speed (1.35 m/s)	-	0.45	0.55	0.42 ± 0.16	0.42 ± 0.16

[a] The difference between this value and the value (0.67 MW) reported in [1] is due to a larger number of iterations performed here vs. there

4. Conclusions and perspective

The effect of the choice of turbulence closure on the CFD prediction of convective heat losses from the Solar Two central receiver has been considered in this paper for a simplified receiver geometry approximated by flat panels, starting from previous work done at Sandia using a 1-equation turbulence closure.

Computed steady state convective losses are ~ 2-3% (1%) of the total power absorbed by the receiver, at high (low) wind speed, depending on the turbulence model chosen. These results are consistent with those of available correlations for rough cylinders, if the macroscopic roughness due to the panel edges is accounted for.

The tubes of which the receiver panels are made, neglected in the present model, should contribute an additional roughness of ~ 200×10^{-5}, but experimental evidence, albeit on pyramidal roughness, suggests that at that roughness level the effect on Nu at high Re should have already saturated [12].

In perspective it should be interesting to develop a more comprehensive CFD model, accounting for the structures above and below the cylinder, as well as testing more sophisticated and accurate turbulence models than RANS type.

References

[1] Christian JM, Ho CK. CFD simulation and heat loss analysis of the solar two power tower receiver. Proceedings of ASME 2012 6th International Conference on Energy Sustainability & 10th Fuel Cell Science, Engineering and Technology Conference (ESFuelCell2012), July 23-26, 2012, San Diego, CA, USA.
[2] SAS IP, Inc, "ANSYS FLUENT User's Guide", version 14.5, 2013.
[3] Spalart PR, Allmaras SR. A one-equation turbulence model for aerodynamic flows. AIAA Paper 92-0439, 1992.
[4] Yakhot V, Smith LM. The renormalization group, the ε-expansion and derivation of turbulence models. J Sci Comput 1992;7:35-61.
[5] Menter FR. Two-equation eddy-viscosity turbulence models for engineering applications. AIAA J 1994;32:269-89.
[6] Menter FR. Review of the shear-stress transport turbulence model experience from an industrial perspective. Int J Comp Fl Dyn 2009;23:305-16.
[7] ul-Haque A, Ahmad F, Yamada S, Chaudhry SR. Assessment of Turbulence Models for Turbulent Flow over Backward Facing Step. Proceedings of the World Congress on Engineering 2007 Vol II WCE 2007, July 2 - 4, 2007, London, U.K.
[8] http://www.cfd-online.com/Wiki/Linear_eddy_viscosity_models .
[9] Davoudabadi P. The Most Accurate and Advanced Turbulence Capabilities. Confidence by Design Workshop Chicago, IL, June 14, 2012. Downloadable from http://www.ansys.com/staticassets/ANSYS/Conference/Confidence/Chicago/Downloads/most-accurate-advanced-turbulence-capabilities.pdf .
[10] Incropera FP, et al.. Foundations of heat transfer (6th edition). Wiley, Singapore, 2013.
[11] Siebers DL, Kraabel JS. Estimating convective energy losses from solar central receivers. SAND 84-8717, April 1984.
[12] Achenbach E. The effect of surface roughness on the heat transfer from a circular cylinder to the cross flow of air. Int. J. Heat Mass Transf. 1977; 20:359-69.
[13] Pacheco JE, Ed.. Final test and evaluation results from the Solar Two project. SAND2002-0120, January 2002.